Residual Normal and Shear Stresses on Different Machining-Finished Surfaces of Martensitic Ultrahigh Strength Steel

Quanshun Luo[1,*], Yubi Gao[1,2] and Yutian Ding[2]

[1]*Materials and Engineering Research Institute, Sheffield Hallam University, Sheffield, S1 1WB, UK*

[2]*State Key Laboratory of Advanced Processing and Recycling of Nonferrous Metals, Lanzhou University of Technology, Lanzhou, Gansu Province, 730050, China*

Abstract: Machining induced residual stresses are known to have influenced mechanical properties of high strength metallic alloys. In this paper, we have compared the surface residual stresses of an ultrahigh strength martensitic/bainitic steel grade 56NiCrMoV7 induced by two different machining processes, namely turning and milling. Using the established $d\sim\sin^2\psi$ method, x-ray diffraction technique was employed to measure the residual stresses on both the axial and hoop directions of cylindrical samples. The results reveal that, turning finish led to tensile residual stress in the axial direction and compressive residual stress in the hoop direction. On the other hand, milling finish led to compressive residual stresses in both the axial and hoop directions. In addition, large splitting in the $d\sim\sin^2\psi$ linear regressions has been interpreted by the presence of residual shear stresses.

Keywords: Residual stresses, Machined surfaces, X-ray diffraction, Shear stresses, High strength steel.

1. INTRODUCTION

Martensitic ultrahigh strength steels are widely used in vehicles and aircrafts to bear heavy loads. Because of the extremely high level of strengthening through several mechanisms, this martensitic structure has reached its maximum strength properties whereas the ductility is restricted to an inferior level. For this reason, the fatigue strength becomes more sensitive to any damage of the surface structure integrity, including the scale and type of surface residual stresses. In particular, poor machining always results in the generation of severe residual stresses along with other types of surface damages. In some extreme cases, it is even difficult to measure the tensile properties of ultrahigh strength steel if a tensile specimen is not properly machined. Figure **1** shows the fractures of two tested tensile bars which were finished by fine turning, manual polishing and by grinding respectively. More details of the research and development of the ultrahigh strength steel can be found in our previous publications [1-3]. The turning-polishing finished sample experienced an unusual fracture during the tensile test following its crack nucleation at the machining-damaged surface edge. The unexpected fracture caused underestimation of the tensile properties, especially the plasticity. On the other hand, the grinding finished sample fractured properly by crack initiation exactly at the geometric centre of the section.

Machining induced surface residual stresses have been studied extensively [4-12]. Such residual stresses can be caused by several factors. Firstly, a cutting edge provides compressive and shear loads to a small volume in front of the cutting edge and leads to both the compressive residual stress along the direction of shear deformation and the tensile residual stress normal to the shearing direction. Secondly, the combined severe plastic deformation heat and frictional heat results in a residual tensile thermal stress. For hardened steels having martensitic microstructure, residual stresses can also be generated as a sequence of thermally induced phase transformation. Xin studied the surface residual stresses of high strength steels after high speed milling and reported residual tensile stresses along axial direction [4]. Zhang reported residual tensile stresses in the surface of turning-machined 300M ultrahigh strength steel [5]. Liu reported residual compressive stresses on the surface of a hardened medium carbon steel induced by grinding [6]. For ultrahigh strength steels, it is important to prevent the generation of residual tensile stresses because such stresses may cause the loss of fatigue resistance.

Another issue for machining induced residual stresses has been the co-existence of normal and shear stresses. It is known that the $d\sim\sin^2\psi$ linear regression method is an important basis of X-ray diffraction (XRD) residual stress measurement [13,14]. Using this method, it is convenient to measure the bi-axial residual stresses of coatings and various strengthened or deformed surfaces. However, the stress calculation is based on the assumptions of in-

*Address correspondence to this author at the Materials and Engineering Research Institute, Sheffield Hallam University, Sheffield, S1 1WB, UK; Tel: 0044 114 2253649; Mobile: 0044 7967302493; Fax: 0044 114 2253501; E-mail: q.luo@shu.ac.uk
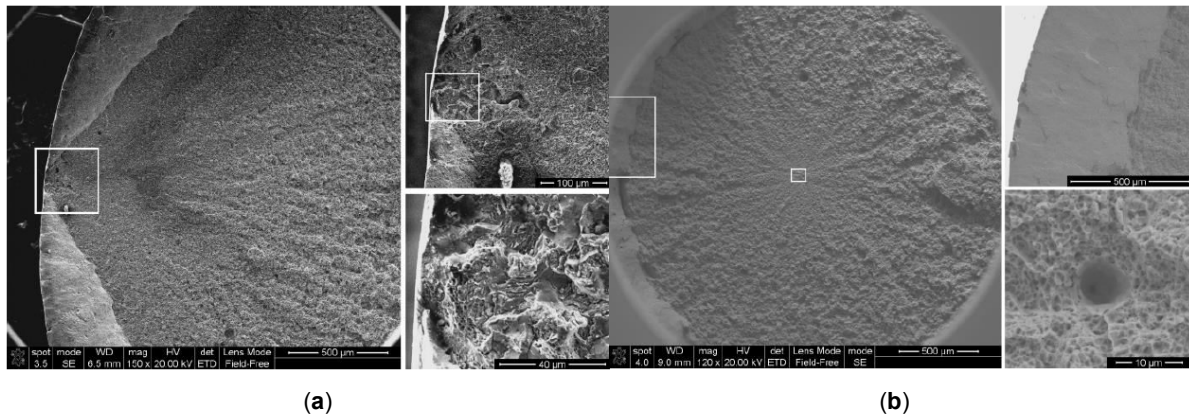
(**a**)   (**b**)

Figure 1: Scanning electron micrographs showing the fracture overview of two tensile bars: (**a**) a sample finished by fine turning and manual polishing; (**b**) a sample finished by grinding.

plane stresses i.e., zero normal stress (vertical to the measured surface) and zero shear stresses. As a result, its applications in measuring machining induced residual stresses may be problematic because of the co-existence of both normal and shear stresses. For example, the existence of residual shear stresses is known to result in splitting in the $d \sim \sin^2 \psi$ linear regression. This phenomenon appears often, but has been addressed rarely in literature.

In this paper, we present the results of XRD residual stress measurements of a grade of ultrahigh strength steel 56NiCrMoV7 to investigate the effect of turning and grinding on the bi-axial residual stresses of cylindrical samples. In addition, an attempt has been made to estimate the residual shear stresses related to the splitting of the obtained $d \sim \sin^2 \psi$ linear regression.

2. EXPERIMENTAL

Samples for the machining tests and residual stress measurements were a grade of hot-rolled alloyed spring steel having nominal compositions (in wt%) of C 0.55, Ni 1.69, Cr 1.05, Mo 0.50, Mn 0.76, Si 0.30, V 0.08, P 0.014, S 0.0037, and iron (Fe) in balance. The steel was hardened to obtain optimal mechanical properties as shown in Table **1**. Before the tensile testing, samples were machined using two types of finishing. One group was finished by fine turning and subsequent manual polishing, whereas another group by grinding. Residual stress measurements were made

on three samples, including two turning-polished finished samples and one grinding finished sample.

An X-ray diffractometer Philips X'Pert was employed for the residual stress measurements, using Cu-Ka radiation (wavelength 0.15406 nm, anode at 40kV and 40 mA). Using the Ω-2θ scan mode, eleven fixed glancing angles at Ω = 9.1° - 70.5° were selected to scan the diffraction peak F(211) in the range 2θ = 80° - 84°, expecting the resultant off-axis angle ψ = -32° - +32°. Given the applied diffraction condition and linear absorption coefficient of Ka-Cu in iron (μ/ρ = 324 cm^2/g), the resultant X-ray depth penetration was between 0.56 - 1.24 µm. In other words, the results presented in this paper are the surface residual stresses in a depth range of 0.56 - 1.24 µm. The scans were made at a step size of 0.026° and sufficiently a long acquisition of time to obtain a maximum peak intensity higher than 1,000 count. All the acquired diffraction data were processed by Ka2 stripping, substrate removing and 9-point smoothening, and then further filtered by Lorentz-Polarisation-Absorption before the diffraction peak measurement. Each diffraction peak was measured using the parabolic approach. The detailed methodology, including the selection of diffraction peak and the data processing, has been demonstrated in our previous research for its high precision [15,16]. For each cylindrical sample, measurements were made in two directions, namely, the axial direction and the hoop direction. Using the measured lattice d-spacing d, derived from the

Table 1: Mechanical Properties of the Sample Steel

Property	HV	Tensile strength, MPa	Yielding strength, MPa	Elongation %	Reduction area, %	V-Notch Charpy, J
Value	693 ± 9	2140 ± 24	1876 ± 107	8.7 ± 1.2	36 ± 2	11 ± 1

diffraction angle 2θ using the Bragg Equation, and the calculated ψ values ($\psi = \theta - \Omega$), the d ~ $\sin^2\psi$ linear regression was performed to calculate the residual stress. The E modulus and Poisson's ratio ν were adapted as 210 GPa and 0.26 respectively.

3. RESULTS

3.1. Residual Stresses of the Turning-Polishing Finished Samples

Figure **2** shows the stress measurement results along the axial direction of the 5-mm turning-polishing finished bar. Figure **2a** is a collection of all the acquired F(211) diffraction peaks, where the peaks for the $\psi > 0$ and $\psi < 0$ positions were drown in thin solid lines and dashed lines respectively. Figure **2b** shows the d-spacing values plotted versus the corresponding $\sin^2\psi$ values. The data exhibit large scale of splitting between the two groups of d ~ $\sin^2\psi$ data, i.e. the data for $\psi > 0$ in the upper part and those for $\psi < 0$ in the lower part. Linear regressions have been made for the overall data, for the $\psi > 0$ group, and for the $\psi < 0$ group respectively, as printed in the chart. The general regression shows a very weak positive slope of 0.00002 and a very low precision coefficient $R^2 = 0.0015$. The low R^2 value was attributed to the ψ splitting instead of measurement error, as the linear regressions for the $\psi > 0$ and $\psi < 0$ groups both exhibit very high R^2 values of 0.94 and 0.96 respectively. Nevertheless, the linear regression turns out to be an estimated residual tensile stress of 29 ± 248 GPa.

Obviously, the large deviation derives from the ψ splitting.

Figure **3** shows the residual hoop stress measurements of the same sample as shown in Figure **2**. It turns out a small compressive stress of -67 ± 64 MPa. Unlike the axial stress measurements, the ψ splitting is quite small, which consequently leads to a small value of deviation ± 64 MPa. Measurements were repeated on another turning machined tensile bar sample. The sample was 7 mm in diameter and was finished by manual polishing. The results of the d ~ $\sin^2\psi$ regressions for the axial and hoop directions are shown in Figure **4**. Again, both measurements show large scales of ψ splitting. The residual stresses at the axial and hoop directions were determined to be 151 ± 233 MPa and -171 ± 139 MPa respectively.

In summary of the measurements, the turning and polishing finished cylindrical samples exhibit a residual tensile stress at axial direction and residual compressive stress along hoop direction. These results are consistent with the measurements published in literature [4, 5, 9]. In these published researches, the authors attributed the residual tensile stresses to several factors, including the compressive loads in front of cutting edge leading to an uneven compressive plastic deformation, and cutting induced heating resulting in localized annealing of martensitic microstructure in the thermally affected layer. Considering the harmful impact on the fatigue
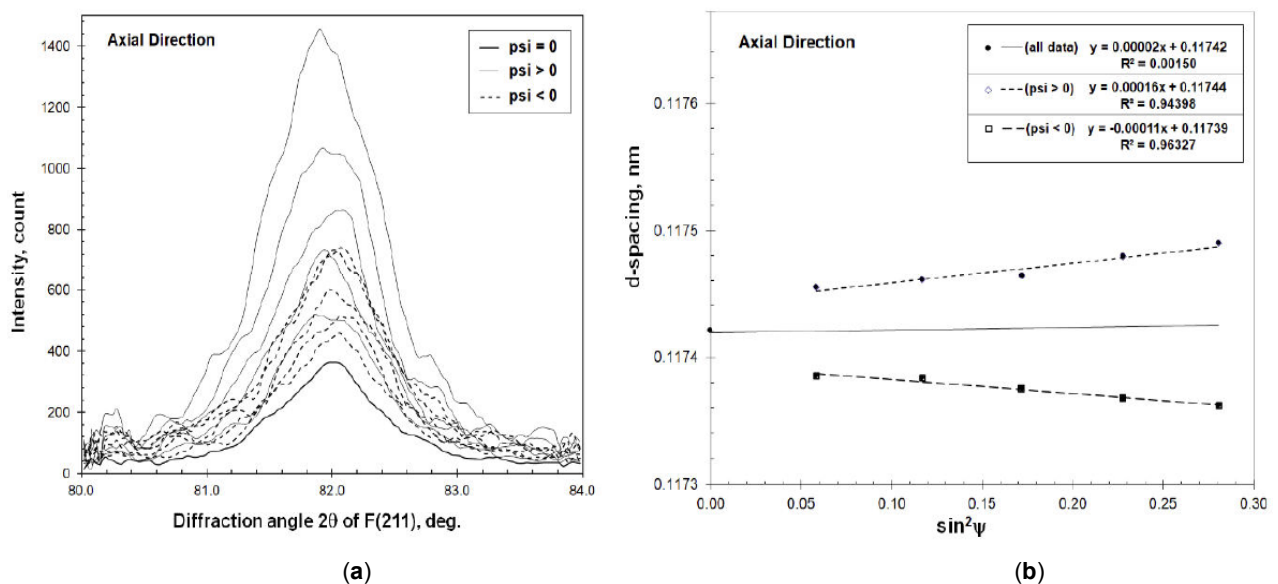

(a)

(b)

Figure 2: Measurement results on the axial direction of the turning-polishing finished 5-mm bar sample: (**a**) the collected diffraction peaks and (**b**) the obtained d ~ $\sin^2\psi$ linear regressions. Note that linear regressions were made for three series of data, namely, for $\psi > 0$, $\psi < 0$, and for all data.
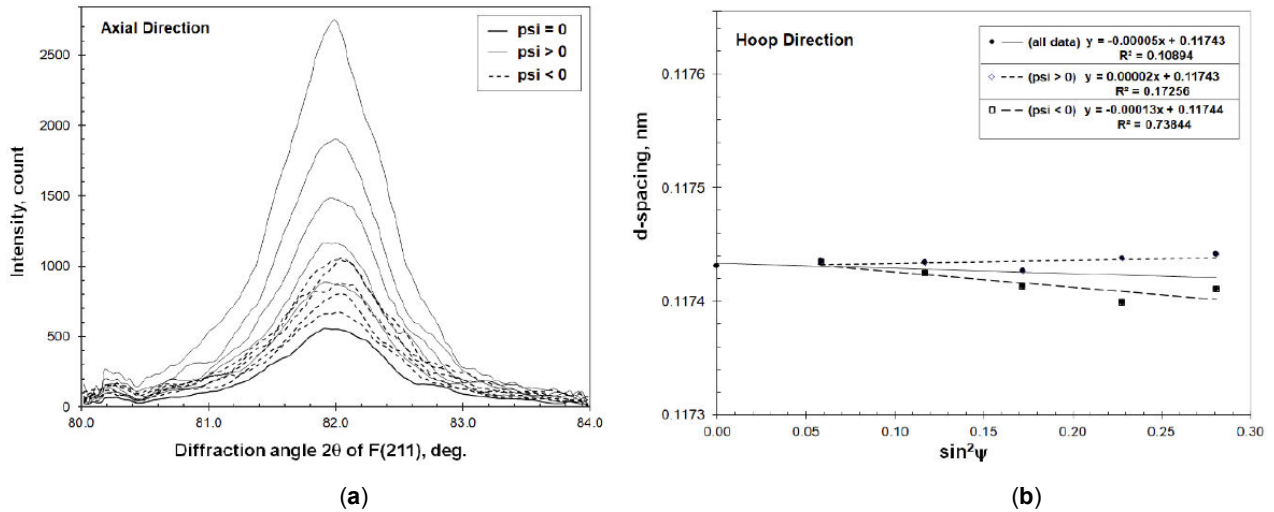
(a)

(b)

Figure 3: Measurement results on the hoop direction of the turning-polishing finished 5-mm bar sample: (**a**) the collected diffraction peaks and (**b**) the obtained $d \sim \sin^2\psi$ linear regressions.
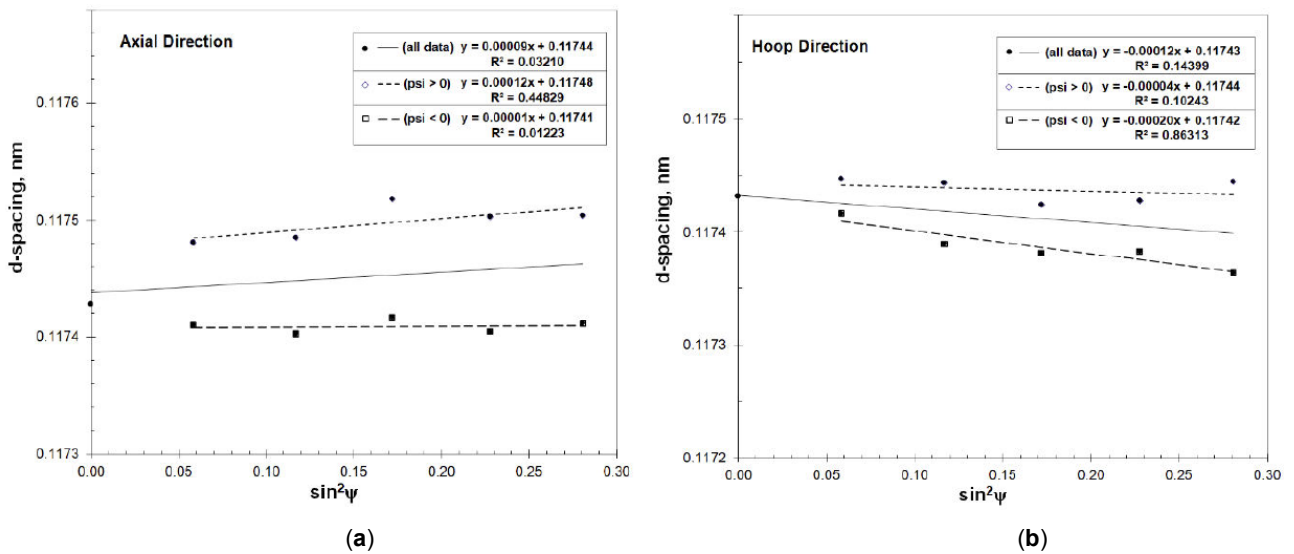

(a)

(b)

Figure 4: The $d \sim \sin^2\psi$ linear regressions of the turning-polishing finished 7-mm bar sample: (**a**) the axial direction, and (**b**) the hoop direction.

resistance of martensitic ultrahigh strength steels, such residual tensile stresses should be prevented.

3.2. Residual Stresses of the Grinding Finished Sample

Figure **5** shows the $d \sim \sin^2\psi$ linear regressions of the grinding finished tensile bar sample. The $d \sim \sin^2\psi$ chart of the axial direction exhibits ψ splitting similar to those presented in Figures **3-4**. In these $d \sim \sin^2\psi$ charts, the d values in the $\psi > 0$ range are larger than those in the $\psi < 0$ range. The $d \sim \sin^2\psi$ chart of the hoop direction differs from these in that, the d values in the $\psi > 0$ range are smaller than those in the $\psi < 0$ range. Nevertheless, the residual stresses at the axial and hoop directions were calculated to be -20 ± 187

MPa and -115 ± 102 MPa respectively, both exhibiting residual compressive stresses.

The measured residual compressive stresses differ from those reported in literature [5,6], in which grinding was observed to cause residual tensile stresses. For the generation of residual stresses in grinding, several important factors have to be considered. A grinding process is accomplished by multiple cutting edges with negative front cutting angles. The negative front angle results in severe plastic deformation and subsequently compressive residual stresses along the cutting direction. Meanwhile, the thermal shock accompanying the high-rate straining, triggers residual tensile stresses. Where the role of these factors is contradictory to each other, the resultant residual
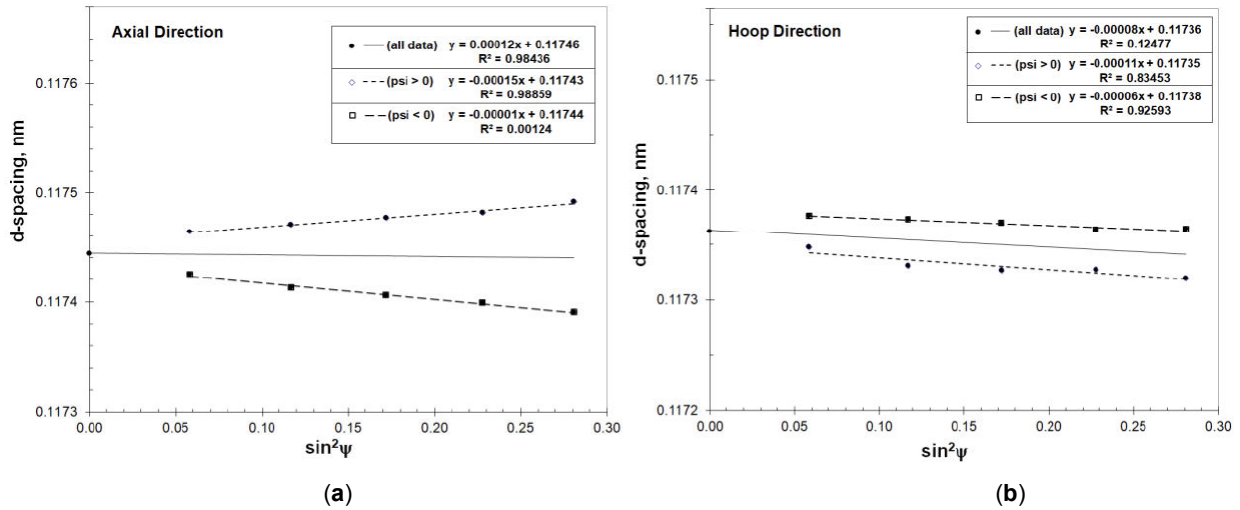
Figure 5: The d ~ sin$^2\psi$ linear regressions of the grinding finished 7-mm bar sample: (**a**) the axial direction, and (**b**) the hoop direction.

stresses are believed to be strongly dependent to the applied grinding condition. In current work, grinding as the finishing cutting generated residual compressive stresses in both directions, which satisfied the need for tensile testing by preventing the unexpected crack nucleation at surface edge, Figure **1b**.

3.3. Consideration of the ψ Splitting

In this work, most of the obtained results showed different scales of ψ splitting. Such ψ splitting does not appear in the d ~ sin$^2\psi$ regressions of thin films and coatings [17-19]. To our knowledge, the phenomenon of ψ splitting has been rarely studied in details in literature except some theoretical analysis [20]. So it is worthwhile to conduct some initial analysis, which we did in this paper. In literature [13,14], ψ splitting was reported to imply the presence of shear stresses in the bi-axial plane and along the bi-axial directions. Here we attempt to develop formula for the calculation of residual shear stresses according to the measured ψ splitting.

The d ~ sin$^2\psi$ method of XRD residual stress measurement derives from the following equation (1), in which ϕ presents an angle in the plane normal to the axis 3, i.e. ϕ = 0° for the axis 1 and ϕ = 90° for the axis 2, seeing Figure **6**. For bi-axial residual stress measurement, i.e., assuming ε_{33} = 0, Equation (1) is re-written as Equation (2).

$$\frac{d_{\phi\psi} - d_0}{d_0} = \left(\varepsilon_{11} \cdot \cos^2 \phi + \varepsilon_{12} \cdot \sin^2 \phi + \varepsilon_{22} \cdot \sin^2 \phi \right)$$
$$\cdot \sin^2 \psi + \varepsilon_{33} \cdot \cos^2 \psi + \varepsilon_{13} \cdot \text{con} \phi \cdot \sin^2 \psi + \varepsilon_{23} \cdot \sin^2 \phi \cdot \sin^2 \psi \qquad (1)$$

$$\frac{d_{\phi\psi} - d_0}{d_0} = \left(\varepsilon_{11} \cdot \cos^2 \phi + \varepsilon_{12} \cdot \sin^2 \phi + \varepsilon_{22} \cdot \sin^2 \phi \right)$$
$$\cdot \sin^2 \psi + \varepsilon_{13} \cdot \text{con} \phi \cdot \sin^2 \psi + \varepsilon_{23} \cdot \sin \phi \cdot \sin^2 \psi \qquad (2)$$

In current work, we define ϕ = 0° for the axial direction and ϕ = 90° for the hoop direction. The Equations (3) and (4) present the resultant formula respectively. Then Equations (5) and (6) can be derived to calculate the shear strains ε_{13} and ε_{23} for a pair of +ψ and -ψ having the same absolute |ψ| value. By adapting a shear modulus G = 79 GPa, we have calculated the shear stresses along the axial and hoop direction. The results are shown in Table **2**.

$$\frac{d_{\phi\psi} - d_0}{d_0} = \varepsilon_{11} \cdot \sin^2 \psi + \varepsilon_{13} \cdot \sin^2 \psi \qquad (3)$$

$$\frac{d_{\phi\psi} - d_0}{d_0} = \varepsilon_{22} \cdot \sin^2 \psi + \varepsilon_{23} \cdot \sin^2 \psi \qquad (4)$$

$$\frac{d_{\psi} - d_{-\psi}}{d_0} = 2 \cdot \varepsilon_{13} \cdot \sin^2 \psi \qquad (5)$$

$$\frac{d_{\psi} - d_{-\psi}}{d_0} = 2 \cdot \varepsilon_{23} \cdot \sin^2 \psi \qquad (6)$$

Equations (5-6) can be interpreted as that, the presence of ψ splitting can be quantified by d_ψ- $d_{-\psi}$≠ 0, and the related shear strains can be quantified for the given ψ value.

4. CONCLUSIONS

Using the XRD d~sin$^2\psi$ method, for measuring machining induced surface residual stresses of an

Table 2:   Summary of the Calculated Normal Stresses (σ) and Shear Stresses (τ)

Sample	Axial, MPa		Hoop, MPa	
	σ	τ	σ	τ
Turning-polishing finished 5 mm dia.	29 ± 248	45 ± 4	-67 ± 64	15 ± 5
Turning-plishing finished 7 mm dia.	151± 233	43 ± 6	-171 ± 139	24 ± 6
Grinding finished 7 mm dia.	-20 ± 187	32 ± 4	-115 ± 102	-19 ± 3

ultrahigh strength steel we have drawn the following conclusions.

1. The tensile bars finished by turning and manual polishing exhibit residual tensile stress in the axial direction and compressive stress in the hoop direction. On the other hand, the grinding finished bar exhibits residual compressive stresses both in the axial and hoop directions.

2. Most of the obtained d~$\sin^2\psi$ regressions show large scales of ψ splitting, implying the machining induced shear stresses.

3. Equations have been developed and applied for calculation of residual shear stresses.

REFERENCES

[1]   Luo Q, Kitchen M, Patel V, Magowan S. Carbon partitioning and structure evolution in the hardening treatments of high strength steel, Proceedings of the 20th Congress of International Federation for Heat Treatment and Surface Engineering, Beijing China, October 23-25, 2012; 111-117.

[2]   Luo Q, Kitchen M, Patel V, Filleul M, Owens D. Partial-isothermally-treated low alloy ultrahigh strength steel with martensitic/bainitic microstructure, Proceedings HSLA Steels 2015, Microalloying 2015 & Offshore Engineering Steels 2015, The Chinese Society for Metals and Chinese Academy of Engineering, November 11-13, 2015, Hangzhou, China, TMS 2016; 433-438.
https://doi.org/10.1007/978-3-319-48767-0_50

[3]   Luo Q, Kitchen M, Abubakri S. Effect of austempering time on the microstructure and carbon partitioning of ultrahigh strength steel 56NiCrMoV7, Metals 2017; 7: No. 258.
https://doi.org/10.3390/met7070258

[4]   Xin M, Xie L, Wang X, Run S, Yang H. Study on the surface residual stress of high hardness and strength alloy steel in high speed milling. Trans Beijing Institute of Technology 2010; 30: 19-23.

[5]   Zhang H, Zhang X, Zhang H, Ren Y, Liu G. Surface quality of high-speed turning 300M ultrahigh strength steel. Surface Technology 2016; 45: 181-187.

[6]   Liu J, Hou D. Study on residual stress in grinding-hardened layer of 40Cr steel. Heat Treatment of Metals 2008; 33: 127-130.

[7]   Madariaga A, Kortabarria A, Hormaetxe E, Garay A, Arrazola PJ. Influence of tool wear on residual stresses when turning Inconel 718. Procedia CIRO 2016; 45: 267-270.
https://doi.org/10.1016/j.procir.2016.02.359

[8]   Jang DY, Watkins TR, Kozaczek KJ, Hubard CR, Cavin OB. Surface residual stresses in machined austenitic stainless steel. Wear 1999; 194: 168-173.
https://doi.org/10.1016/0043-1648(95)06838-4

[9]   Arrazola PJ, Kortabarria A, Madariaga A, Esnaola JA, Fernandez E, Cappellini C, Ulutan D, Özel T. On the machining induced residual stresses in IN718 nickel-based alloy: experiments and prediction s with finite element simulation. Simulation Modelling Practice and Theory 2014; 41: 87-103.
https://doi.org/10.1016/j.simpat.2013.11.009

[10]   Ghosh S, Rana VPS, Kain V, Mittal V, Baveja SK. Role of residual stresses induced by industrial fabrication on stress corrosion cracking susceptibility of austenitic stainless steel. Materials and Design 2011; 32: 3823-3831.
https://doi.org/10.1016/j.matdes.2011.03.012

[11]   Zhang W, Fang K, Hu Y, Wang S, Wang X. Effect of machining-induced surface residual stress on initiation of stress corrosion cracking in 316 austenitic stainless steel. Corrosion Science 2016; 108: 173-184.
https://doi.org/10.1016/j.corsci.2016.03.008

[12]   Ma Y, Feng P, Zhang J, Wu Z, Yu D. Prediction of surface residual stress after end milling based on cutting force and temperature. Journal of Materials Processing Technology 2016; 235: 41-48.
https://doi.org/10.1016/j.jmatprotec.2016.04.002

[13]   Withers PJ, Bhadeshia HKDH. Overview: Residual stress Part 1 - Measurement techniques. Materials Science Technology 2001; 17: 355-365.
https://doi.org/10.1179/026708301101509980

[14]   Cullity BD, Stock SR. Elements of x-ray diffraction, 3rd edition, Upper Saddle River, NJ : Prentice Hall, 2001; p. 435.

[15]   Luo Q, Jones AH. High-precision determination of residual stress of polycrystalline coatings using optimised XRD-sin2ψ technique. Surface and Coatings Technology 2010; 205: 1403-1408.
https://doi.org/10.1016/j.surfcoat.2010.07.108

[16]   Luo Q, Yang S. Uncertainty of the X-ray diffraction (XRD) sin2ψtechnique in measuring residual stresses of physical vapor deposition (PVD) hard coatings. Coatings 2017; 7: No 128.
https://doi.org/10.3390/coatings7080128

[17]   Moreno CM, Sanchez JM, Ardila LC, Aldareguia JMM. Determination of residual stresses in cathodic arc coatings by means of the parallel beam glancing X-ray diffraction technique. Thin Solid Films 2009; 518: 206-22.
https://doi.org/10.1016/j.tsf.2009.07.011

[18]   Teixeira V, Andritschky M, Fischer W, Buchkremer HP, Stover D. Effects of deposition temperature and thermal cycling on residual stress state in zirconia-based thermal barrier coatngs. Surface and Coatings Technology 1999; 120-121: 103-111.
https://doi.org/10.1016/S0257-8972(99)00341-2

[19]   Liu H, Xu Q, Zhang X, Wang C, Tang B. Residual stress analysis of TiN film fabricated by plasma immersion ion

implantation and deposition process Nuclear Instruments and Methods in Physics Research B 2013; 297: 1-6.
https://doi.org/10.1016/j.nimb.2012.12.015

[20] Welzel U, Ligot J, Lamparter P, Vermeulen AC, Mittemeijer EJ. Stress analysis of polycrystalline thin filmsa and surface regions by X-ray diffraction. Journal of Applied Crystallography 2005; 38: 1-29.
https://doi.org/10.1107/S0021889804029516